(This is a sample cover image for this issue. The actual cover is not yet available at this time.)

Earth and Planetary Science Letters 331-332 (2012) 305–314

Contents lists available at SciVerse ScienceDirect

Earth and Planetary Science Letters

journal homepage: www.elsevier.com/locate/epsl

Multiple episodes of fluid flow in the SW Barents Sea (Loppa High) evidenced by gas flares, pockmarks and gas hydrate accumulation

S. Chand [a,*], T. Thorsnes [a], L. Rise [a], H. Brunstad [b], D. Stoddart [b], R. Bøe [a], P. Lågstad [c], T. Svolsbru [d]

[a] Geological Survey of Norway (NGU), P.O. Box 6315 Sluppen, 7491 Trondheim, Norway
[b] Lundin Petroleum Norge AS, Lysaker, Norway
[c] Norwegian Defence Research Establishment (FFI), P.O. Box 25, 2027 Kjeller, Norway
[d] Norwegian Defence Research Establishment (FFI), P.O. Box 115, 3191 Horten, Norway

ARTICLE INFO

Article history:
Received 7 December 2011
Received in revised form 9 March 2012
Accepted 13 March 2012
Available online xxxx

Editor: P. Shearer

Keywords:
pockmarks
gas flares
gas hydrate
Barents Sea
BSR
seismic

ABSTRACT

Gas and gas hydrates have gained considerable attention in the last 20 yr due to their possible impact on global climate change from methane escalations. Our study area, the SW Barents Sea, is unique in its evolution due to the effect of glaciations which removed thick layers of sediment from the seabed. Unloading due to erosion and deglaciation resulted in opening of pre-existing faults and creation of new ones, facilitating fluid migration and eventually escape into the water from the subsurface. Expressions of hydrocarbon gas accumulation and fluid flow such as gas hydrates and pockmarks are widely distributed in the Barents Sea. Several gas flares, some of them 200 m high in echograms, occur along a segment of the Ringvassøy Loppa Fault Complex, indicating open fractures and active fluid flow. Observation of gas flares along regional fault complexes outside pockmark regions indicates that present gas escape occurs along faults only. The pockmark formation and gas flares belong to different episodes of fluid flow. The pockmarks are absent outside soft sediment depocentres indicating that their existence is related to the presence of recording medium. The thin sediment cover in pockmarks and their penetration down into glaciomarine sediments indicate that they formed after deposition of these sediments and that fluid escape was active to the very recent past. Methane hydrate stability zone (MHSZ) modelling shows that after the last glacial maximum 18000–20000 ^{14}C years ago, the MHSZ has thinned from 600 m to zero in most parts of the SW Barents Sea. The fluid expulsion probably happened after retreat of the glaciers causing release of methane from dissociation of methane hydrates through fluid escape processes which lasted until recently. Bottom simulating reflectors (BSR) observed are probably due to structure II hydrates formed from gas containing higher order hydrocarbon components such as ethane, propane, etc. along with methane. The study area falls close to the new gigantic oil discoveries, Skrugard and Havis, and north of the Snøhvit hydrocarbon field.

1. Introduction and geological setting

Fluid flow processes have been proposed to bring large quantities of greenhouse gases such as methane from the deeper geo-sphere to the water column (Pohlman et al., 2010) and to the atmosphere which could cause global scale climate change (Hansen et al., 2000; Shakova et al., 2010). Methane is a green house gas causing 23 times more effect than CO_2 (Forster et al., 2007). Locating the occurrences of gas flares and quantifying the discharge of CH_4 from the seabed and its fate in the water column are still a very new area of research (Reeburgh, 2007). Also, methane emissions are observed to have effects on seabed morphology and benthic ecosystems (Judd et al., 1997). The morphology and nature of the cold seeps worldwide vary significantly from one area to the other, reflecting different mechanisms of fluid generation and tectonic or the stratigraphic frameworks creating fluid pathways (Klaucke et al., 2008; Linke et al., 2010; Naudts et al., 2006).

Many areas of active seepage are associated with sub-seafloor oil and gas reservoirs, trapped gas under gas hydrates, and also dissociation of gas hydrate itself (Milkov and Sassen, 2003; Sassen et al., 1999). Numerous gas flares were identified along the Arctic shelf associated with changes in gas hydrate stability conditions (Westbrook et al., 2009) and focussed fluid flow (Hustoft et al., 2009). Occurrences of gas hydrates in marine areas are often associated with the presence of a bottom simulating reflector (BSR) (Shipley et al., 1979). A BSR is a seismic reflector, representing the base of the gas hydrate stability zone (BGHSZ), and described as one which sub-parallels the seafloor reflection, but which is opposite in polarity (Shipley et al., 1979). The BSR indicates an acoustic impedance change across a high velocity layer of gas hydrate bearing sediments overlying a gas rich layer (Stoll and Bryan, 1979). The nature and properties of BSRs and their occurrences vary depending on the sedimentary environment and fluid flow (Chand and Minshull, 2003; Hobro et al., 2005; Westbrook et al., 2008).

* Corresponding author.
E-mail address: shyam.chand@ngu.no (S. Chand).

0012-821X/$ – see front matter © 2012 Elsevier B.V. All rights reserved.
doi:10.1016/j.epsl.2012.03.021

In many parts of the world BSR depths are altered by the presence of one or more gas hydrate inhibitors (NaCl, N_2, warm fluids, isostatic uplift, deglaciation, sliding) or facilitators (CO_2, H_2S, higher order hydrocarbon gases, increase in sea level, subsidence) (Sloan, 1990). This may result in BSRs occurring at different depths. The detection of BSRs is also complicated due to their variation in properties depending on the frequency used for data acquisition and the type of acoustic boundary formed at the BGHSZ (Vanneste et al., 2001). Often the BGHSZ is controlled by the presence of permeable layers and the presence of a BSR is limited to locations where such layers cross cut the BGHSZ.

The study area lies in the southwestern part of the epi-continental Barents Sea. Mesozoic and early Cenozoic sedimentation in the Barents Sea took place in intracratonic basins. After the early Tertiary opening of the Norwegian Sea, the sediment transport bypassed these basins, and depocentres were established on the continental margin (Spencer et al., 1984). Results from drilling and coring show that erosion took place during the glacial–interglacial periods in the late Plio-Pleistocene (<2.7 Ma) creating the upper regional unconformity (URU) (Solheim and Kristoffersen, 1984). The corresponding sediments hence have a glacial affinity (Eidvin and Riis, 1989; Hald et al., 1990; Sættem et al., 1992). Estimates show that about 1000 m of sediments may have been removed during this erosional episode (Laberg et al., 2011; Nøttvedt et al., 1988; Riis and Fjeldskaar, 1992). An upper glacigenic sediment sequence of varying thickness covers the URU (Solheim and Kristoffersen, 1984). Associated with erosion and isostatic rebound from deglaciation, considerable late Cenozoic uplift took place, modelled by Riis and Fjeldskaar (1992) to be 900–1400 m in the western Barents Sea. The removal of overburden and later uplift resulted in the opening of many pre-existing faults and creation of pathways for fluid flow (Nøttvedt et al., 1988).

Previous studies from the Barents Sea have indicated patchy high amplitude reflections, which are interpreted as BSRs (Andreassen and Hansen, 1995; Chand et al., 2008; 2009; Laberg et al., 1998). They are interpreted to be due to the presence of structure II gas hydrates containing a few percentages of higher order hydrocarbon gases or CO_2 along with methane (Chand et al., 2008; Laberg et al., 1998). Modelling has shown that pure methane hydrates cannot be stable where these anomalies occur. A similar study carried out along the western flank of Ingøydjupet indicated patchy subsurface reflections which again are not conform to pure methane hydrate (Chand et al., 2009). No drilling has been carried out for hydrate sampling along the Barents Sea margin, but a surface gravity core from the Nordkapp Basin indicated presence of hydrate nodules which vaporised when exposed to atmospheric conditions (Chand et al., 2008).

The present study is focussed on a small region along the southwestern Barents Sea covering parts of the western margin of the Hammerfest Basin, the Loppa High, Tromsøflaket and Ingøydjupet. It is close to the new gigantic oil discoveries, Skrugard and Havis, and north of the Snøhvit hydrocarbon field (Figs. 1 and 2). The study is aimed to achieve a better understanding of fluid flow processes and their relation to shallow geological and seabed conditions created by the Plio-Pleistocene erosion/deposition processes and tectonic activity in this region.

2. Materials and methods

Multibeam echosounder (MBE) data were collected by the Norwegian Defence Research Establishment (FFI) using Kongsberg Maritime EM710 mounted on FFI's research vessel HU Sverdrup II (Fig. 1). It is a $0.5\times1.0^{\circ}$ system with operating frequency of 70–100 kHz. With typical water depths of ca 350 m in the study area the MBE data gives 1 to 2 m spatial resolution for the terrain model. The MBE data also include seafloor reflection (backscatter) properties, which indirectly gives an indication of sediment type/grain size and hardness/ruggedness of the seabed. The EM710 system can also record the water column which is very useful for detecting gas bubbles in the water column (gas flares). The EM710 data were processed using Fledermaus Geocoder for backscatter and Fledermaus Midwater for water column gas anomalies.

A parametric subbottom profiler seismic system mounted on HU Sverdrup II, (Kongsberg Defence Systems TOPAS PS18) was used to

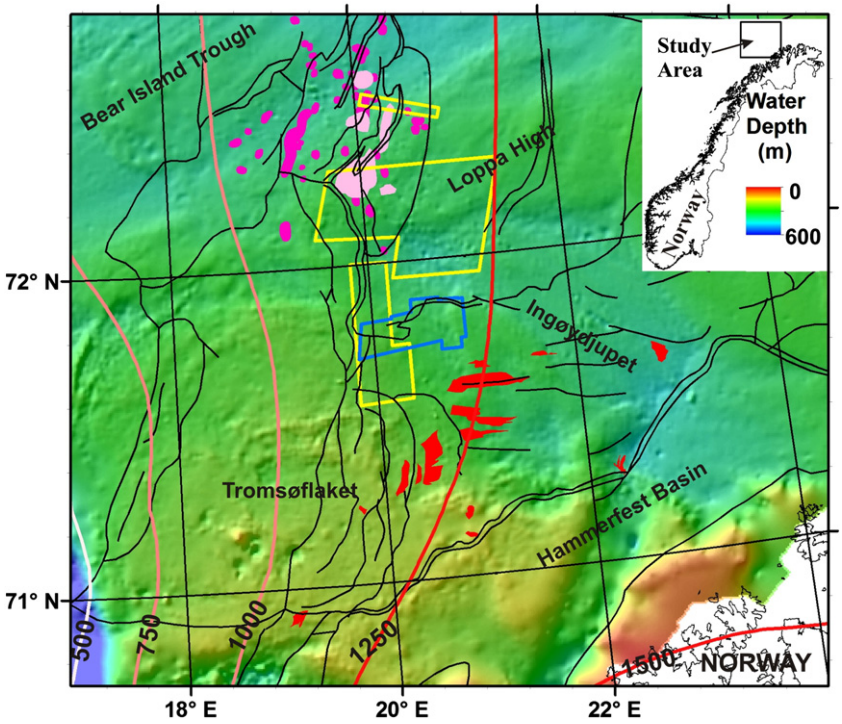

Fig. 1. Regional bathymetry of the Barents Sea showing the location of multibeam bathymetry (yellow polygons) and the 3D seismic block (blue polygon). Also shown are gas anomalies (purple), BSRs (pink) (Andreassen and Hansen, 1995), hydrocarbon discoveries (red), faults (black lines) (Gabrielsen et al., 1990) and ice thickness contours from the Last Glacial Maximum (Siegert et al., 2001). (For interpretation of the references to colour in this figure legend, the reader is referred to the web version of this article.)

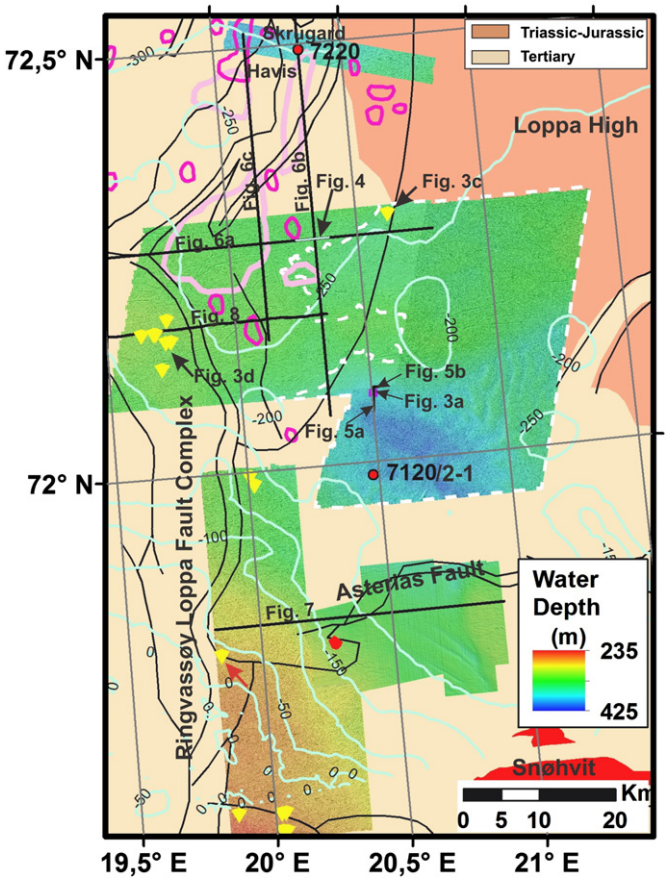

Fig. 2. Detailed bathymetry of the study area overlaid on the structure and bedrock map. Also shown are gas flares (yellow triangles), gas hydrate stability zone depths (light blue contours), boundary of pockmark area (white dashed polygon), BSR occurrences (pink polygons), gas anomalies (purple polygons) (Andreassen and Hansen, 1995), locations of faults (thin black lines) (Gabrielsen et al., 1990), wells (red dots), hydrocarbon fields (red filled polygons), flare connected to subsurface gas anomalies (red arrow) and locations of figures. (For interpretation of the references to colour in this figure legend, the reader is referred to the web version of this article.)

acoustically map the sediments in the uppermost part of the seabed. Sedimentary layering can be clearly imaged giving a detailed stratigraphy over the past few tens of thousands of years. An EdgeTech 2200 high resolution full spectrum chirp sub-bottom profiler (SBP) mounted on FFI's AUV HUGIN, operated from HU Sverdrup II was used to map interesting areas of the immediate subsurface in very high resolution. The HUGIN was flown ~10 m above the seafloor at a constant speed giving 50 cm horizontal resolution and vertical resolution of less than 100 μs (~10 cm) with the SBP system. 2D high resolution seismic using one airgun and an analogue parallel streamer were used to collect single channel seismic data from part of the study area. This gave deeper penetration than the TOPAS seismic, thus linking the near surface to the shallow subsurface. The 2D seismic is limited in usability up to the first multiple which is around 900 ms TWT in our study area. Conventional industry multichannel 2D seismic data covering the study area and the nearby region were available as well as a 3D seismic data cube, LHS08M01 (Fig. 1), from southern part of the study area.

Present thickness of the methane hydrate stability zone (MHSZ) for the Barents Sea was modelled using a modified version of the gas hydrate stability modelling programme CSMHYD (Chand et al., 2008; Sloan, 1990). A smooth bathymetry model available for the whole southwestern Barents Sea (Fig. 1), heat flow values (Bugge et al., 2002) and measured bottom water temperature values (World Ocean Database, WOD, 2005) were used to predict the present MHSZ thickness. MHSZ thickness during the last glacial maximum was modelled using ice thickness models (Fig. 1) proposed for this area (Siegert et al., 2001) and ice (glaciers on the seabed) bottom temperature of 0 °C. The gas hydrate stability zone (GHSZ) thickness for a gas composition of 96% methane, 3% ethane and 1% propane was calculated using the same environmental parameters (Fig. 2).

3. Interpretation and modelling

3.1. Water column, seafloor and shallow stratigraphy

The area mapped by EM710 is located on a broad ridge where water depths range from 235 m to 425 m, with the deepest part to the east (Fig. 2). Iceberg plough marks can be observed crisscrossing the whole area except where they are totally covered by soft sediments. The seabed has varying hardness indicated by variations in backscatter. The deepest areas have comparatively low reflectance, caused by a soft sediment cover. The range of backscatter values observed for the whole study area is very limited, indicating that the sediments are almost uniform, or that at least the shallowest few centimetres of the seafloor are draped by similar kind of sediments with minor changes associated with plough marks and pockmarks.

Pockmarks occur almost exclusively in the deepest part of the study area between 340 and 425 m water depth. The pockmarks are circular, generally less than 35 m in diameter and up to 2 m deep, with an average density of about 150 pockmarks per square kilometre (Fig. 3a). The pockmarks are either randomly distributed, or occur in arrays sometimes associated with iceberg plough marks. There is little variation in size and density of pockmarks, but an about 1 km broad boundary zone of the pockmark area exhibits smaller and shallower pockmarks with lower density. The size (both depth and diameter) of the pockmarks is observed to decrease towards the boundary of the pockmark area. The pockmarks are also smaller in size where the top soft sediment appears to be thinnest. They have higher backscatter values than the surrounding sediments (Fig. 3b) indicating a coarser or harder substrate.

Large, irregular depressions of up to 300 m in diameter, 25 m deep, and with wall slopes of up to 30° occur randomly in the study area (Fig. 3a). They may have irregular shapes, and iceberg plough marks occasionally start/terminate in these depressions, while others have no obvious relation to plough marks. The depressions are draped by marine and glaciomarine sediments of similar thickness to the surrounding seafloor. Some of the depressions contain pockmarks (Fig. 3a). Backscatter values in the depressions are similar to outside of the depressions, but also here pockmarks have higher backscatter (Fig. 3b).

The use of hydroacoustic water column data brought a new dimension to the study of subsurface fluid flow through the detection of acoustic gas flares. Analyses indicate 16 acoustic gas flares in the 2700 km^2 area covered by MBE (Fig. 2). The majority occur outside the pockmark areas. The flares are as high as 200 m (Fig. 3d). One flare is located in the pockmark area close to a branch of the Ringvassøy Loppa Fault Complex (RLFC) (Figs. 2 and 3c).

The TOPAS and airgun data show the general character of sediments above the Upper Regional Unconformity (URU) and those underlying it (Fig. 4). High amplitude anomalies can be seen close to the seafloor both in TOPAS and airgun data indicating the presence of gas (Fig. 4). The data cannot resolve the structure of pockmarks due to the lower frequency used. On the contrary, the very high resolution SBP data give detailed images of pockmarks and subsurface stratigraphy (Fig. 5a). Pockmarks are observed to cut across glaciomarine reflectors a few milliseconds below the seafloor indicating that they formed after the end of glaciomarine sedimentation (Fig. 5a). Glaciomarine deposits underlying the pockmarks appear to be little influenced by their formation, indicating that they generally formed by seeping of fluids (Fig. 5a). Pockmarks are almost barren

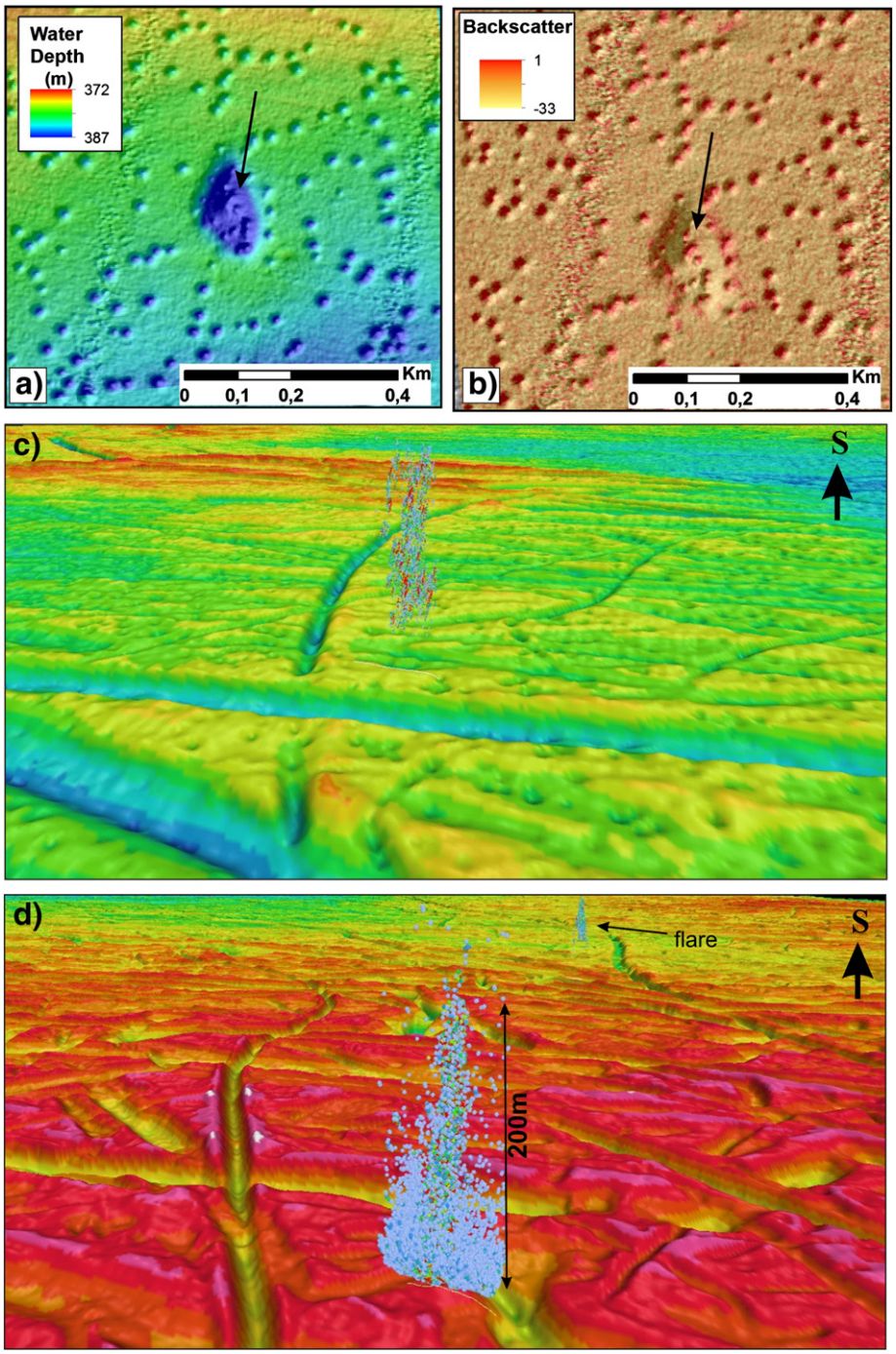

Fig. 3. a) Bathymetry and b) backscatter datasets showing the structure and backscatter properties of pockmarks and depressions. Notice the occurrence of pockmarks within depressions. Gas flares from c) pockmark area and d) non pockmark area shown on shaded relief bathymetry. Notice that the flares occur from iceberg plough marks. See Fig. 2 for location.

in the case of marine sediments implying fluid flow activity until the very recent past (Fig. 5a and b). The glaciomarine sediments appear as stratified layers indicating clear boundaries within the sediments (Fig. 5a and b). These high-reflective layers could be the reason for the high backscatter observed at the centre of these pockmarks. The depressions are observed to have infill of both marine and glaciomarine sediments indicating that these features formed before the deposition of glaciomarine sediments (Fig. 5a). The tills underlying the depressions appear to be disturbed, indicating that they could be features formed by iceberg plunging on the seafloor creating iceberg prodmarks. It is also possible that they may have formed by explosive expulsion of fluids prior to the deposition of the glaciomarine succession, but this is regarded as less likely for the majority of these features (Fig. 5a).

3.2. Deep seismic stratigraphy and basin structure

Airgun seismic data indicate marine/glaciomarine sediment thicknesses of up to 10 ms TWT covering underlying till (Fig. 6a and b). The URU can be seen crosscutting pre-glacial formation boundaries and bedding older than 2.7 Ma (Fig. 6a and b). Amplification of reflectors and phase reversal is observed in glacial and preglacial sediments, reflecting captured gas along bedding and stratigraphic boundaries (Fig. 6a, b and c). The predicted BGHSZ crosscuts the

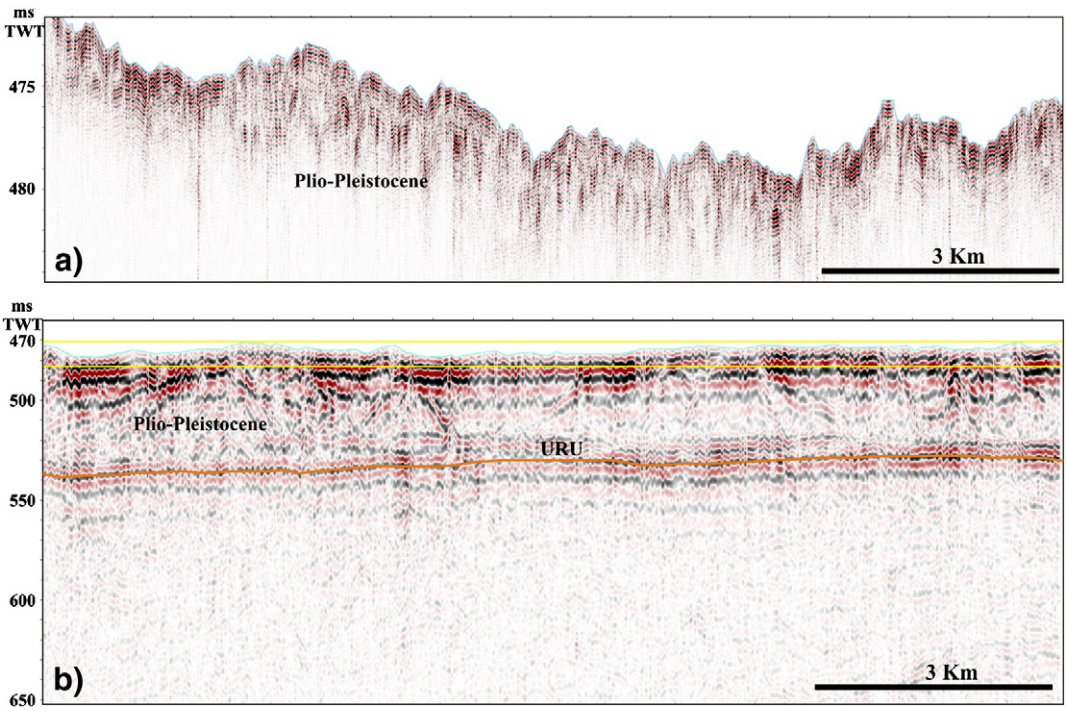

Fig. 4. a) TOPAS and b) airgun seismic sections outside the pockmark area. The TOPAS data give high resolution image of the seafloor which is covered by only one wavelet in the airgun data set. See Fig. 2 for location.

dipping bedding and many pockets of high amplitudes can be noticed at this level (Fig. 6a and b).

Glacial and postglacial deposits are around 50–150 ms TWT thick in the study area. Preglacial sediment units pinch out against the Loppa High with less than 100 ms TWT sediment thickness overlying the Tertiary succession (Fig. 6). BSRs are observed close to the predicted BGHSZ depths as patchy, high amplitude reflections (Fig. 6a and b). They occur close to stratigraphic boundaries but are truncated. This

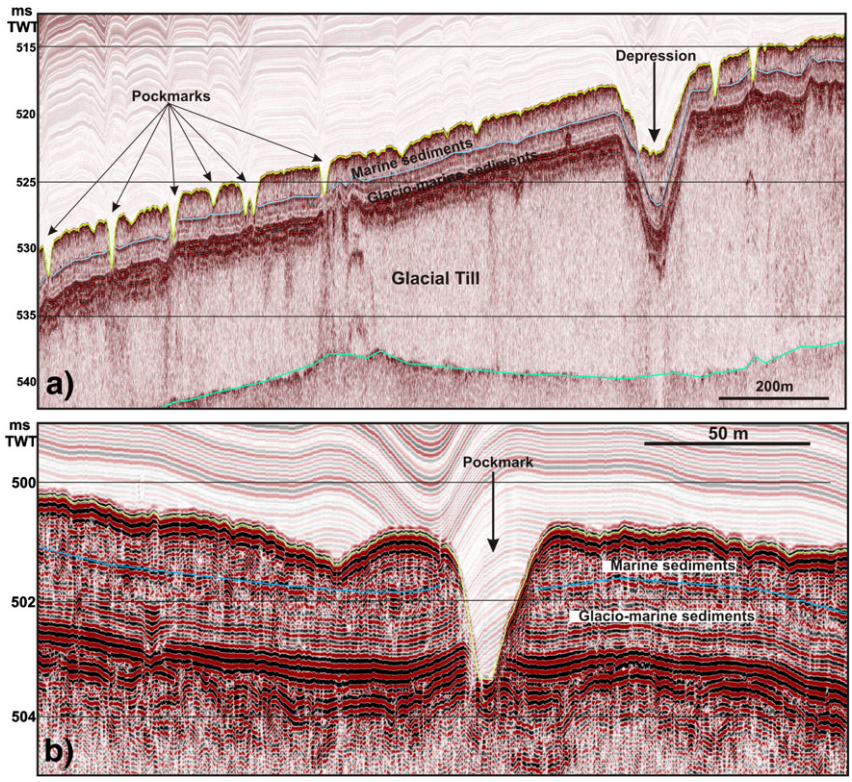

Fig. 5. a) High resolution SBP line across the pockmark area showing subsurface sedimentary structure of the pockmarks and depressions. Notice that the depression is infilled with marine and glaciomarine sediments while pockmarks look fresh with very little marine sediments. b) High resolution SBP image of pockmark showing that they have very little marine sediments deposited. The pockmark is cutting across the marine–glaciomarine boundary (blue line) indicating that they formed after the deposition of glaciomarine sediments. See Fig. 2 for location. (For interpretation of the references to colour in this figure legend, the reader is referred to the web version of this article.)

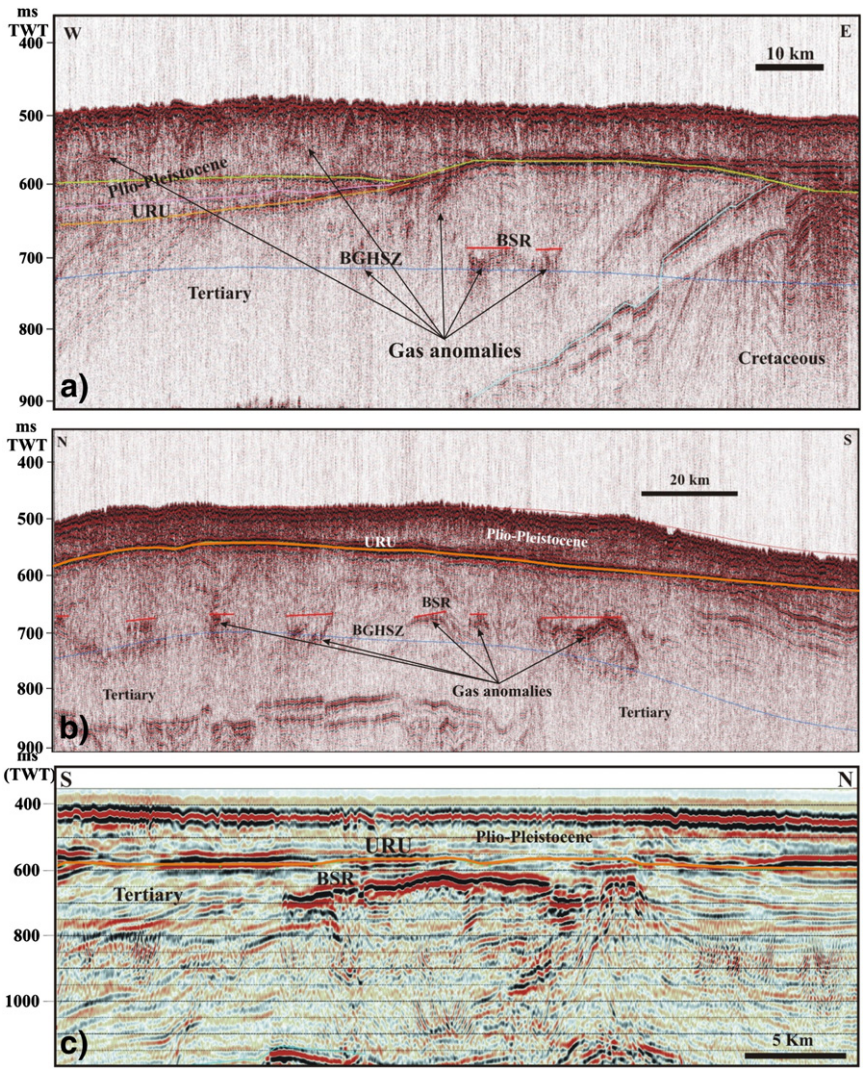

Fig. 6. a) 2D airgun seismic line in W–E direction and b) N–S direction indicating gas anomalies below the URU (orange line) close to the base of the gas hydrate stability zone (blue line) (BGHSZ). The anomalies have flat tops and do not follow the bedding. The anomalies follow the seafloor topography and are very close to the BGHSZ. c) 2D multichannel seismic line showing a major high amplitude reflection (BSR) sub-paralleling the seafloor. The anomaly falls close to the predicted BSR depth. Also shown is the URU (orange line). See Fig. 2 for location. (For interpretation of the references to colour in this figure legend, the reader is referred to the web version of this article.)

indicates a limited lateral extent due to lack of open pathways for gas supply (Fig. 6a). Industry multichannel 2D seismic data indicate strong and continuous BSRs compared to the localised and weak BSR anomalies observed in high resolution airgun data (Fig. 6c). This shows the strong frequency dependency of the BSR reflector. The 3D seismic data along the southern part of the study area were also interpreted for possible gas/BSR anomalies. Gas anomalies and fluid pathways along westerly dipping stratigraphic layers can be clearly noticed (Fig. 7). The 3D seismic data also indicate similar anomalies at various depths focussed towards the Loppa high. A comparison of near and far offset data indicates that these anomalies are due to gas (Fig. 7). One of the flares occurs where these anomalies meet the seafloor (Fig. 2). No clear BSR-like reflection is identified in the 3D seismic data. Regional seismic cross sections across the study area where most of the gas flares occur indicate that the subsurface formations that flank the Loppa high are highly faulted (Fig. 8).

Seismic interpretation of the post-Cretaceous section based on 2D seismic lines covering the study area shows the general architecture west of the Loppa High (Fig. 9). The seismic stratigraphy indicates shallowing from all directions towards the Loppa High at all stratigraphic levels. The base Cretaceous horizon shallows towards the Loppa High (Figs. 8a and 9a) and terminates below the Tertiary close to the western boundary of the study area. The main BSR anomaly lies close to the termination of the base Cretaceous reflector beneath the URU (Fig. 9a). The base Tertiary reflector terminates at the Loppa High but only a very thin section of Tertiary sediments overlies Jurassic sediments (Fig. 9b). Quaternary sediments overlying the URU follow the general basin architecture with deeper URU away from the Loppa High (Fig. 9c). A deep channel occurs at the URU level midway between the 3D seismic area and the study area indicating deeper erosion by glaciers there (Fig. 9c). The shallowing of all stratigraphic boundaries and confinement as a basin is prominent close to the termination of the base Cretaceous reflector leading to focussed fluid flow (Fig. 9a, b and c).

3.3. Gas hydrate stability zone: past and present

The base of the regional MHSZ for the Barents Sea is estimated at a depth from 0 to 250 m below seafloor, depending on the present day bathymetry and bottom water temperature (Fig. 10a). It is inferred from modelling that a more than 1200 m thick ice cap covered the SW Barents Sea during the last glacial maximum, about 18000–20000 ^{14}C years ago (Siegert et al., 2001). This made the whole SW Barents Sea stable for methane hydrate with MHSZ depths up to 600 m below the present seafloor (Fig. 10b). The difference between the present MHSZ and that during last glacial maximum

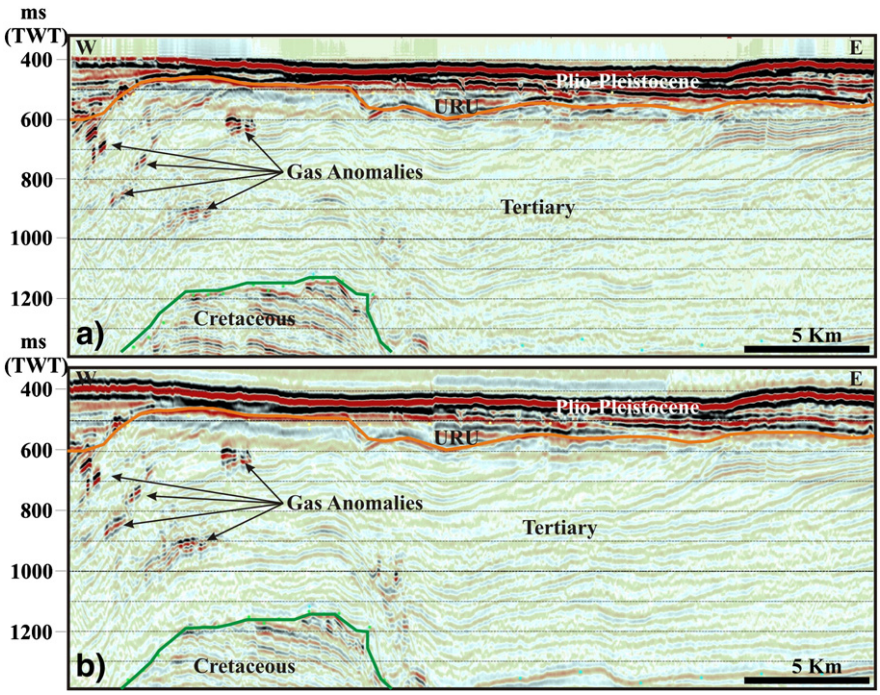

Fig. 7. a) Near offset and b) far offset data of 3D seismic cube showing gas anomalies at various levels along the layering. The accumulation of gas upslope of the westward dipping beds along permeable layers indicate a focussing mechanism towards the crest of the Triassic domal structure while open faults allow cross formation fluid flow. See Fig. 2 for location.

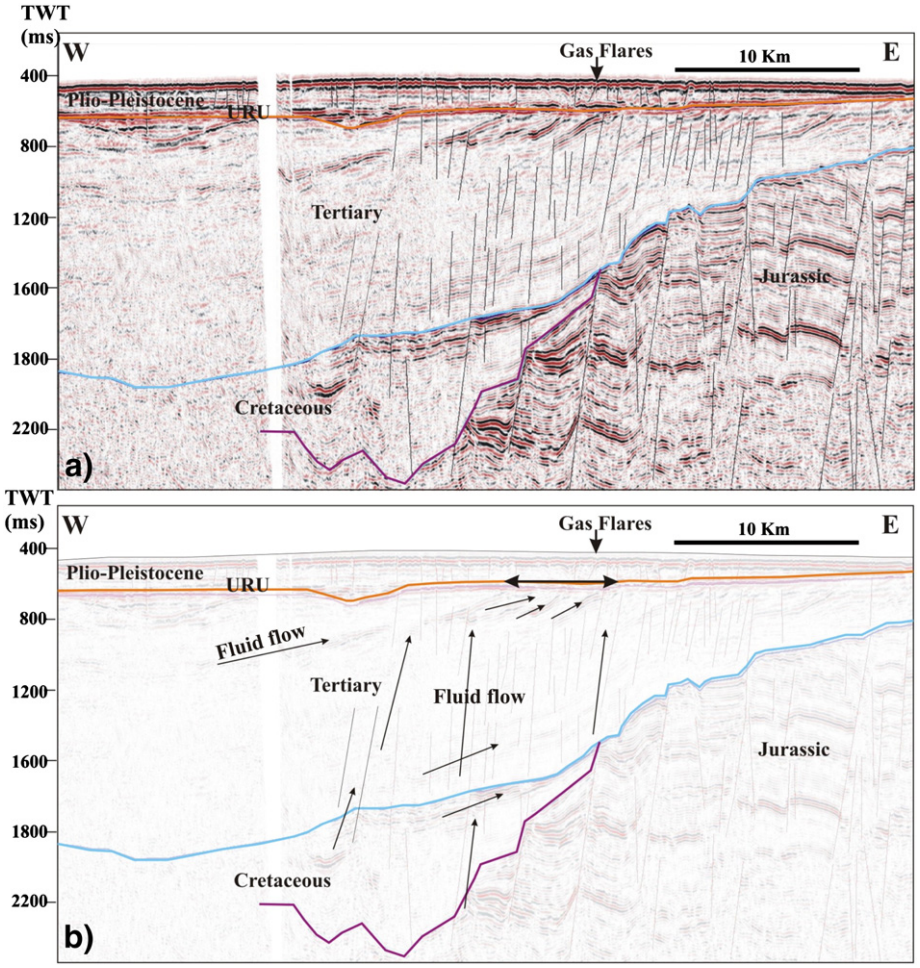

Fig. 8. a) Seismic section and b) subsurface geology and fluid flow model which focus fluids towards gas flares observed at the seafloor. The fluids are transported along intra-Tertiary permeable formations and along the base of the Tertiary sediments while highly fractured Tertiary and Cretaceous sediments allow fluid flow through open faults. Notice the large amount of fracturing in the Plio-Pleistocene allowing fluid flow through glacial till. See Fig. 2 for location.

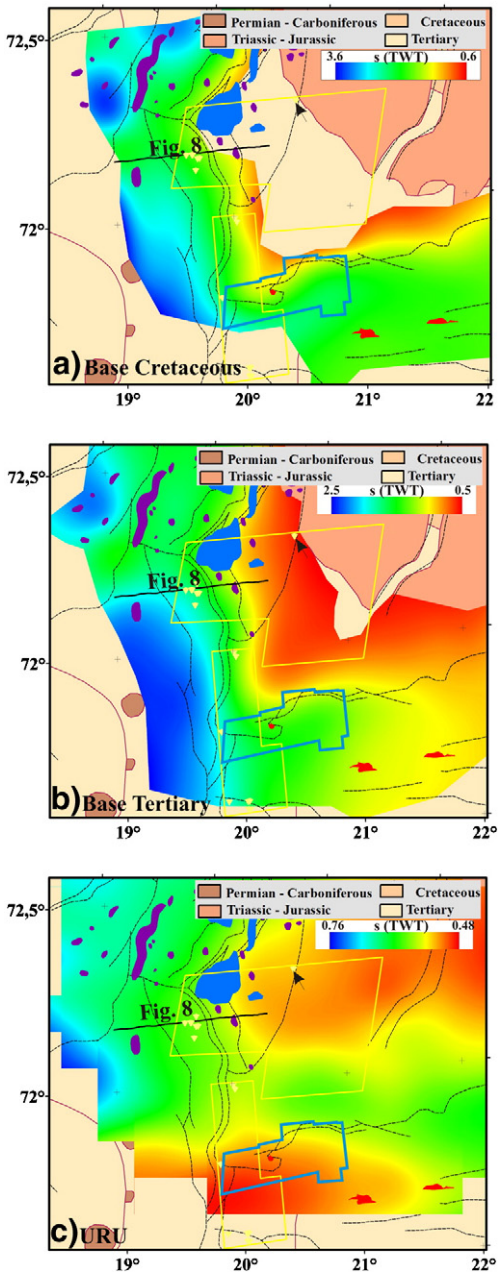

Fig. 9. Two way time depths (seconds) to a) base Cretaceous, b) base Tertiary and c) URU superimposed on structural and bedrock map of the region. Also shown are locations of multibeam bathymetry and 3D seismic dataset (blue polygon), faults (thin black lines), gas flares (yellow triangles), gas indications (purple) and BSRs (blue). The majority of the gas flares occur along the Ringvassøy Loppa Fault Complex (RLFC) while one flare occurs in the pockmark area (indicated by black arrow) close to a branch of the fault in the NNE direction. (For interpretation of the references to colour in this figure legend, the reader is referred to the web version of this article.)

indicates a change of thickness by up to 600 m. The MHSZ within the Bear Island trough thinned to less than 250 m while most of the other parts of the south western Barents Sea including our study area lie outside the MHSZ. The major change occurred outside the Bear Island trough making this region prone to release of methane accumulated during the last glaciation as methane hydrates. The present regional gas hydrate stability estimated for structure II hydrates (96% methane, 3% ethane and 1% propane) for the Barents Sea indicates a ~250 m deep BGHSZ covering the study area where the MHSZ is zero (Chand et al., 2008). The estimated two way travel time (TWT) thickness to the BGHSZ is around 220–270 ms assuming 1990 m/s velocity for the sediments (observed at well 7220) (Fig. 2).

4. Fluid flow: present and past

The Barents Sea is a region reported to have a large number of open faults due to the removal of overburden by glaciers and the resulting uplift (Nøttvedt et al., 1988). The Barents Sea region excluding the Bear Island Trough is outside the methane hydrate stability field (structure I) due to shallow water depth (Chand et al., 2008). This results in formation of only structure II gas hydrates where higher order hydrocarbon gases or CO_2 are present along with methane (Chand et al., 2008). The extra requirement for the presence of higher order hydrocarbon gases caused hydrates to form as patches wherever stability conditions are met but making it difficult to identify due to the lack of clear BSRs. The BSRs may also have shifted from the general BGHSZ depths due to influx of warm or salty fluids from below through open faults, altering gas hydrate stability conditions (Holbrook et al., 2002; Hustoft et al., 2009). In such places, high amplitude reflections below and above gas hydrate stability depths could be due to gas hydrate patches which might be misinterpreted as gas anomalies.

The structural geometry with enclosed basins and subsurface formations onlapping the Loppa high provide good conditions for focussed fluid flow. This is similar to other gas hydrate provinces offshore Norway. For example, the gas hydrate related BSRs along the Vøring Basin are located along the periphery of the Helland Hansen Arch (Chand et al., 2011). Fluids from deeper formations are suggested to follow permeable formations along the domal structure and are released to the seafloor through pipe like structures (Chand et al., 2011). The fluid flow in the Vøring Basin is also controlled by the extent of less permeable glacial debris (Chand et al., 2011). Where glacial debris covers the crest of the Helland Hansen Arch and further offshore, no pockmarks occur (Buenz et al., 2003; Chand et al., 2011). Chand et al. (2011) suggested build up of overpressure in oozes and focussed fluid flow creating weak surfaces facilitating slope failure. The pockmarks there are reported to be less active (Chen et al., 2010; Ivanov et al., 2010; Vaular et al., 2010) and no gas flares have been reported. On the contrary, along the Vestnesa Ridge, offshore Svalbard, pockmarks with active flares are observed along the crest of a sedimentary drift which has a thick MHSZ. Hustoft et al. (2009) attributed the pockmarks and gas flares to focussing of fluids along the slope through subsurface permeable formations within the sedimentary package. The warm fluids are bringing gas to the seafloor piercing the gas hydrate stability zone up to the seafloor.

The western flank of the Loppa High (Fig. 9) has a structure similar to the Vøring Margin, where older formations are flanking on to a structural high, thereby causing upslope fluid flow. No pockmarks are observed at the gas flares indicating that the region is devoid of any soft sediments. The gas flares are observed only along the RLFC (Fig. 2) indicating that they are associated with these regional faults. The absence of gas flares in the main pockmark areas suggest that they probably formed from fluid escape at the end of the last deglaciation. Comparison of the marine/glaciomarine boundary depth with data from the JM05-085-GC gravity core in the deeper part of Ingøydjupet~90 km away (Aagaard-Sørensen et al., 2010) indicates that the topmost reflector cross cut by the pockmarks is ca 13240 ^{14}C years old (Fig. 5). The study area was suggested to be free from grounded ice at 15790 ^{14}C years BP (Junttila et al., 2010). The glaciomarine sediments underlying these pockmarks are undisturbed indicating that they formed through a slow process of fluid escape rather than explosive release of gas. It can be noticed from the SBP data that most of the pockmarks cut across glaciomarine sediment layers suggesting their formation after the deposition of these sediments.

The presence of both inactive pockmarks and active acoustic gas flares probably demonstrate the two different processes which took place after the glaciers retreated from this area. The first process was probably the release of gas held as methane hydrates and

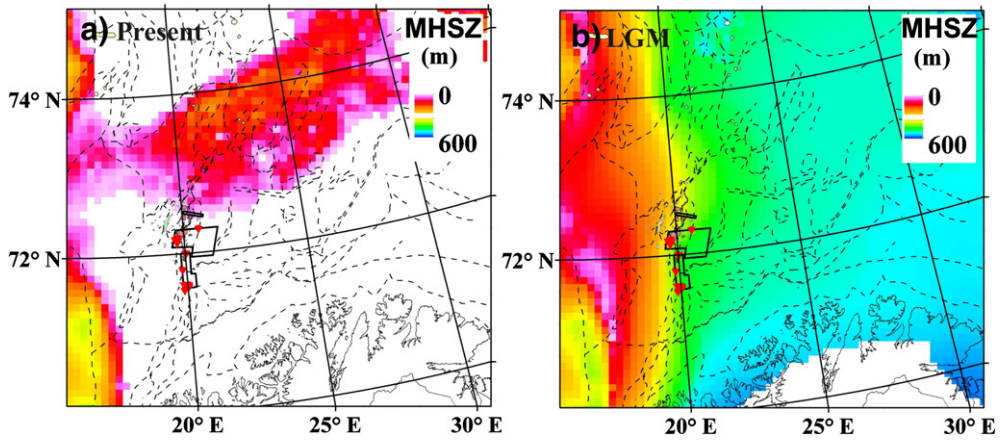

Fig. 10. a) Present and b) LGM methane hydrate stability zones (MHSZ) thicknesses for south western Barents Sea estimated using bathymetry data, heat flow data (Bugge et al., 2002), bottom water temperature data (World Ocean Database, WOD, 2005) and ice thickness (Siegert et al., 2001). Notice the big change in MHSZ thickness since LGM along our study area. Also shown are the gas flares (red triangles) and locations of MBB data (black polygons).

under it after the fast deposition of glaciomarine sediments when the seafloor temperature increased causing the release of gas charged fluids creating the pockmarks. The gas flares observed along the regional faults represent the second process where the present fluid escape occurs through focussed fluid flow along stratigraphic boundaries facilitated by the presence of open faults. This probably was initiated by the slow isostatic uplift and fracturing of the tills.

5. Conclusions

1. The detailed bathymetry and backscatter data show typical signatures of pockmarks with circular to oval shapes and high backscatter at their centres indicating coarse grained sediments.
2. Pockmarks only occur where soft sediments can act as recording medium.
3. BSR-like anomalies sub-paralleling the seafloor occur as patchy reflections. Gas hydrate stability modelling indicates stability of structure II gas hydrates with a few percent of hydrocarbon gases.
4. Similarity of subsurface structures between this area and other fluid flow provinces indicates focussed fluid flow along stratigraphic boundaries and leakage through open faults.
5. The presence of both inactive pockmarks and active acoustic gas flares point towards a two stage development. After the glaciers retreated from the area followed by fast deposition of glaciomarine sediments, the pockmarks formed due to the dissociation of gas hydrates. The acoustic gas flares located along the regional faults belong to fluid flow associated with isostatic uplift and opening up of faults.
6. The identification of so many flares along a comparatively small area, in a short segment of a regional fault complex (RLFC), covering less than 1% of the regional fault complexes of the SW Barents Sea, indicates that there could be many more gas flares yet to be identified.

Acknowledgement

We thank Lundin Norge AS for financial support and data access. We also thank the Norwegian Defence Research Establishment (FFI) and the crew of HU Sverdrup for collecting the data. Petrel software provided by Schlumberger was used for seismic interpretation and visualisation. Vista Seismic Processing package provided by GEDCO was used processing high resolution SBP data. We thank the journal referees, Jens Greinert and Giuliana Rossi, for providing useful comments and suggestions which helped in improving the manuscript.

References

Aagaard-Sørensen, S., Husum, K., Hald, M., Knies, J., 2010. Paleoceanographic development in the SW Barents Sea during the Late Weichselian–Early Holocene transition. Quat. Sci. Rev. 29, 3442–3456.
Andreassen, K., Hansen, T., 1995. Inferred gas hydrates offshore Norway and Svalbard. Norsk Geologisk Tidskrift 45, 10–34.
Buenz, S., Mienert, J., Berndt, C., 2003. Geological controls on the Storegga gas hydrate system of the mid Norwegian continental margin. Earth Planet. Sci. Lett. 209, 291–307.
Bugge, T., Elvebakk, G., Fanavoll, S., Mangerud, G., Smelror, M., Weiss, H.M., Gjelberg, J., Kristensen, S.E., Nilsen, K., 2002. Shallow stratigraphic drilling applied in hydrocarbon exploration of the Nordkapp Basin, Barents Sea. Mar. Pet. Geol. 19, 13–37.
Chand, S., Minshull, T.A., 2003. Seismic constraints on the effects of gas hydrate on sediment physical properties and fluid flow: a review. Geofluids 3, 275–289.
Chand, S., Mienert, J., Andreassen, K., Knies, J., Plassen, L., Fotland, B., 2008. Gas hydrate stability zone modelling in areas of salt tectonics and pockmarks of the Barents Sea suggest an active hydrocarbon venting system. Mar. Pet. Geol. 25, 625–636.
Chand, S., Rise, L., Ottesen, D., Dolan, M.F.J., Bellec, V., Bøe, R., 2009. Pockmark like depressions near the Goliat hydrocarbon field, Barents Sea: morphology and genesis. Mar. Pet. Geol. 26, 1035–1042.
Chand, S., Rise, L., Knies, J., Haflidason, H., Hjelstuen, B.O., Bøe, R., 2011. Stratigraphic development of the south Vøring margin (Mid-Norway) since early Cenozoic time and its influence on subsurface fluid flow. Mar. Pet. Geol. doi:10.1016/j.marpetgeo.2011.01.005.
Chen, Y., Ussler III, W., Haflidason, H., Lepland, A., Hovland, M., Rise, L., Hjelstuen, B.O., 2010. Sources of methane inferred from pore water $\delta^{13}C$ of dissolved inorganic carbon in pockmark G11, offshore mid Norway. Chem. Geol. 275, 127–138.
Eidvin, T., Riis, F., 1989. Nye dateringer av de tre vestligste borehullene I Barentshavet. Resultater og konsekvenser for den tertiaere hevingen. NPD Contribution, 27. 44 pp.
Forster, P., Ramaswamy, V., Artaxo, P., Berntsen, T., Betts, R., Fahey, D.W., Haywood, J., Lean, J., Lowe, D.C., Myhre, G., Nganga, J., Prinn, R., Raga, G., Schulz, M., Van Dorland, R., 2007. Changes in atmospheric constituents and in radiative forcing. In: Solomon, S., et al. (Ed.), Climate Change 2007: The Physical Science Basis. Contribution of Working Group I to the Fourth Assessment Report of the Intergovernmental Panel on Climate Change. Cambridge University Press.
Gabrielsen, R.H., Færseth, R.B., Jensen, L.N., Kalheim, J.E., Riis, F., 1990. Structural elements of the Norwegian Continental Shelf Part I: the Barents Sea Region. NPD Bulletin No. 6. 47 pages.
Hald, M., Saettem, J., Nesse, E., 1990. Middle and Late Weichselian stratigraphy in shallow drillings from the southwestern Barents Sea: foraminiferal, amino acid and radiocarbon evidence. Nor. Geol. Tidskr. 70, 241–257.
Hansen, J., Sato, M., Ruedy, R., Lacis, A., Oinas, V., 2000. Global warming in the twenty-first century: an alternative scenario. Proc. Natl. Acad. Sc. U. S. A. 97, 9875–9880.
Hobro, J.W., Minshull, T.A., Singh, S.C., Chand, S., 2005. A three dimensional seismic tomographic study of the gas hydrate stability zone, offshore Vancouver Island. J. Geophys. Res. 110, B09102. doi:10.1029/2004JB003477.
Holbrook, W.S., Gorman, A.R., Hornbach, M., Hackwith, K.L., Nealon, J., 2002. Seismic detection of marine methane hydrate. Lead. Edge 686–689.
Hustoft, S., Buenz, S., Mienert, J., Chand, S., 2009. Gas hydrates in mounded contourites; implications on focussed fluid migration at the western Svalbard margin. Earth Planet. Sci. Lett. 284, 12–24.
Ivanov, M., Mazzini, A., Blinova, V., Kozlova, E., Laberg, J.-S., Matveeva, T., Taviani, M., Kaskov, N., 2010. Seep mounds on the Southern Vøring Plateau (offshore Norway). Marine and Petroleum Geology 27, 1235–1261.
Judd, A., Davies, G., Wilson, J., Holmes, R., Baron, G., Bryden, I., 1997. Contributions to atmospheric methane by natural seepages on the U.K. continental shelf. Mar. Geol. 140, 427–455.

Junttila, J., Aagard_Sørensen,, S., Husum, K., Hald, M., 2010. Late Glacial-Holocene clay minerals elucidating glacial history in the SW Barents Sea. Mar. Geol. 276, 71–85.
Klaucke, I., Petersen, C.J., Masson, D.G., Weinrebe, W., Ranero, C.R., 2008. Multifrequency geoacoustic imaging of fluid escape features offshore Costa Rica: implications for the quantification of seep processes. Geochem. Geophys. Geosys. 9, Q04010. doi:10.1029/2007GC001708.
Laberg, J.S., Andreassen, K., Knutsen, A.M., 1998. Inferred gas hydrate on the Barents shelf — a model for its formation and a volume estimate. Geo-Mar. Lett. 18, 26–33.
Laberg, J.S., Andreassen, K., Knies, J., Vorren, T.O., Winsborrow, M., 2011. Late Pliocene–Pleistocene development of the Barents Sea Ice Sheet. Geol. Soc. Am. 38, 107–110.
Linke, P., Sommer, S., Rovelli, L., McGinnis, D.F., 2010. Physical limitations of dissolved methane fluxes: the role of bottom-boundary layer processes. Mar. Geol. 272, 209–222.
Milkov, A.V., Sassen, R., 2003. Preliminary assessment of resources and economic potential of individual accumulations in the Gulf of Mexico continental slope. Mar. Pet. Geol. 20, 111–128.
Naudts, L., Greinert, J., Artemov, Y., Staelens, P., Poort, J., Van Rensbergen, P., De Batist, M., 2006. Geological and morphological setting of 2778 methane seeps in the Dnepr paleo-delta, northwestern Black Sea. Mar. Geol. 227, 177–199.
Nøttvedt, A., Berglund, T., Rasmussen, E., Steel, R., 1988. Some aspects of Tertiary tectonics and sediments along the western Barents shelf. In: Morton, A.C., Parson, L.M. (Eds.), Early Tertiary volcanism and the opening of the NE Atlantic: Geological Society of London, special publication, 39, pp. 421–425.
Pohlman, J.W., Bauer, J.E., Waite, W.F., Osburn, C.L., Chapman, N.R., 2010. Methane hydrate-bearing seeps as a source of aged dissolved organic carbon to the oceans. Nat. Geosci. 4. doi:10.1038/NGEO1016.
Reeburgh, W.S., 2007. Oceanic methane biogeochemistry. Chem. Rev. 107, 486–513.
Riis, F., Fjeldskaar, W., 1992. On the magnitude of the late tertiary and quaternary erosion and its significance for the uplift of Scandinavia and the Barents Sea. In: Larsen, R.M., Brekke, H., Larsen, B.T., Talleraas, E. (Eds.), Structural and Tectonic Modelling and its Application to the Petroleum Geology NPF Special Publication 1. Elsevier, Amsterdam, pp. 163–185.
Sættem, J., Rise, L., Westgaard, D.A., 1992. Composition and properties of glacigenic sediments in the southwestern Barents Sea. Mar. Geotechnol. 10, 229–255.
Sassen, R., Joye, S., Sweet, S.T., DeFreitas, D., Milkov, A.V., MacDonald, I.R., 1999. Thermogenic gas hydrates and hydrocarbon gases in complex chemosynthetic communities, Gulf of Mexico continental slope. Org. Geochem. 30, 485–497.
Shakova, N., Semiletov, I., Salyuk, A., Yusupov, V., Kosmach, D., Guustafsson, O., 2010. Extensive methane venting to the atmosphere from sediments of the East Siberian Arctic Shelf. Science 327, 1246–1250.
Shipley, T.H., Houston, M., Buffler, R.T., Shaub, F.J., McMillan, K.J., Ladd, J.W., Worzel, J.L., 1979. Seismic reflection evidence for the wide spread occurrence of possible gas hydrate horizons on continental slopes and rises. AAPG 63, 2204–2213.
Siegert, M.J., Dowdeswell, J.A., Hald, M., Svendsen, J.I., 2001. Modelling the Eurasian Ice sheet through a full (Weichselian) glacial cycle. Glob. Planet. Change 31, 367–385.
Sloan, E.D., 1990. Clathrate Hydrates of Natural Gases. Marcel Dekker, NewYork.
Solheim, A., Kristoffersen, Y., 1984. Sediments above the upper regional unconformity: thickness, seismic stratigraphy and outline of the glacial history. Nor. Polar. Skr. 179B, 26.
Spencer, A.M., Home, P.C., Berglund, L.T., 1984. Tertiary structural development of western Barents shelf: Troms to Svalbard. In: Spencer, A.M. (Ed.), Petroleum Geology of the North European Margin. Graham and Trotman, London, pp. 199–210.
Stoll, R.D., Bryan, G.M., 1979. Physical properties of sediments containing gas hydrates. J. Geophys. Res. 84, 645–648.
Vanneste, M., Batist, M.De., Gomshtok, A., Kremlev, A., Versteeg, W., 2001. Multi-frequency seismic study of gas hydrate bearing sediments in Lake Baikal, Siberia. Mar. Geol. 172, 1–21.
Vaular, E.N., Barth, T., Haflidason, H., 2010. New insights on fluid flow at Nyegga pockmark field (Norwegian Sea) with isotope values from gas hydrate in the G11 pockmark. Org. Geochem. 41, 437–444.
Westbrook, G.K., Chand, S., Rossi, G., Long, C., Buenz, S., Camerlenghi, A., Carcione, J.M., Dean, S., Foucher, J.P., Flueh, E., Gei, D., Haacke, R.R., Madrussani, G., Mienert, J., Minshull, T.A., Nouze, H., Peacock, S., Reston, T.J., Vanneste, M., Zilmer, M., 2008. Estimation of gas hydrate concentration from multicomponent seismic data at sites on the continental margins of NW Svalbard and the Storegga region of Norway. Mar. Pet. Geol. 25, 744–758.
Westbrook, G.K., Thatcher, K.E., Rohling, E.J., Piotrowski, A.M., Palike, H., Osborne, A.H., Nisbet, E.G., Minshull, T.A., Lanoiselle, M., James, R.H., Huhnerbach, V., Green, D., Fisher, R.E., Crocker, A.J., Chabert, A., Bolton, C., Beszczynska-Moller, A., Berndt, C., Aquilina, A., 2009. Escape of methane gas from the seabed along the West Spitsbergen continental margin. Geophys. Res. Lett. 36, L15608. doi:10.1029/2009GL039191.
World Ocean Database (WOD), 2005. http://www.nodc.noaa.gov/General/temperature.html.